Article

Development of radioiodinated benzofuran derivatives for in vivo imaging of prion deposits in the brain

Takeshi Fuchigami, Masao Kawasaki, Ryusuke Koyama, Mari Nakaie, Takehiro Nakagaki, Kazunori Sano, Ryuichiro Atarashi, Sakura YOSHIDA, Mamoru Haratake, Masahiro Ono, Noriyuki Nishida, and Morio Nakayama

ACS Infect. Dis., **Just Accepted Manuscript** • DOI: 10.1021/acsinfecdis.8b00184 • Publication Date (Web): 15 Mar 2019

Development of radioiodinated benzofuran derivatives for *in vivo* imaging of prion deposits in the brain

Takeshi Fuchigami,[†] Masao Kawasaki,[†] Ryusuke Koyama,[†] Mari Nakaie,[†] Takehiro Nakagaki,[‡] Kazunori Sano,[§] Ryuichiro Atarashi,[∥] Sakura Yoshida,[†] Mamoru Haratake,[⊥] Masahiro Ono, ^ Noriyuki Nishida,[‡] Morio Nakayama[†]

[†] Department of Hygienic Chemistry, Graduate School of Biomedical Sciences, Nagasaki University, 1-14 Bunkyo-machi, Nagasaki 852-8521, Japan

[‡] Department of Molecular Microbiology and Immunology, Graduate School of Biomedical Sciences, Nagasaki University, 1-12-4 Sakamoto, Nagasaki 852-8523, Japan

[§] Department of Physiology and Pharmacology, Faculty of Pharmaceutical Sciences, Fukuoka University, 8-19-1 Nanakuma, Jonan-ku, Fukuoka, Japan.

[∥] Department of Infectious Diseases, Faculty of Medicine, University of Miyazaki, 5200 Kihara, Kiyotake, Miyazaki 889-1692, Japan.

[⊥] Faculty of Pharmaceutical Sciences, Sojo University, 4-22-1 Ikeda, Kumamoto 860-0082, Japan

^ Graduate School of Pharmaceutical Sciences, Kyoto University, 46-29 Yoshida Shimoadachi-cho, Sakyo-ku, Kyoto 606-8501, Japan

Corresponding Authors:

Takeshi Fuchigami, E-mail: t-fuchi@nagasaki-u.ac.jp.

Morio Nakayama, E-mail: morio@nagasaki-u.ac.jp.

Prion diseases are fatal neurodegenerative disorders associated with the deposition of abnormal prion protein aggregates (PrP^{Sc}) in the brain tissue. Here, we report the development of ^{125}I-labeled iodobenzofuran (IBF) derivatives as single photon emission computed tomography (SPECT) imaging probes to detect cerebral PrP^{Sc} deposits. We synthesized and radioiodinated several 5-IBF and 6-IBF derivatives. The IBF derivatives were evaluated as prion imaging probes using recombinant mouse prion protein (rMoPrP) aggregates and brain sections of mouse-adapted bovine spongiform encephalopathy (mBSE)-infected mice. Although all the IBF derivatives were strongly adsorbed on the rMoPrP aggregates, [^{125}I]5-IBF-NHMe displayed the highest adsorption rate and potent binding affinity with an equilibrium dissociation constant (K_d) of 12.3 nM. Fluorescence imaging using IBF-NHMe showed clear signals of the PrP^{Sc}-positive amyloid deposits in

the mBSE-infected mouse brains. Biodistribution studies in normal mice demonstrated slow uptake and clearance from the brain of ^{125}I-IBF derivatives. Among the derivatives, [^{125}I]6-IBF-NH_2 showed the highest peak brain uptake [2.59% injected dose (ID)/g at 10 min] and good clearance (0.51% ID/g at 180 min). Although the brain distribution of IBF derivatives should still be optimized for *in vivo* imaging, these compounds showed prospective binding properties to PrP^{Sc}. Further chemical modification of these IBF derivatives may contribute to the discovery of clinically applicable prion imaging probes.

KEYWORDS: Prion disease, PrP^{Sc}, benzofuran, single photon emission computed tomography (SPECT)

Prion diseases, also known as transmissible spongiform encephalopathies, are fatal neurological disorders that affect humans and animals.[1-2] The hallmarks of these diseases include abnormal prion protein accumulation in the brain, spongy vacuolation, and severe neuronal loss.[3] Prion diseases have the unique characteristic of being induced by infectious or inherent factors, or both. Bovine spongiform encephalopathy (BSE) in cattle and chronic wasting disease (CWD) in deer are known as animal prion diseases. Human prion diseases have been classified into Creutzfeldt-Jakob disease (CJD), Gerstmann-Sträussler-Scheinker syndrome (GSS), fatal familial insomnia (FFI), and kuru.[4-5] Misfolding of the normal cellular prion protein PrP (PrP^{C}) into pathogenic scrapie PrP (PrP^{Sc}) is considered to play a key role in the disease progression.[6] Although PrP^{C} has a predominantly α-helix structure, PrP^{Sc} is rich in β-sheet content and has propagating properties.[7] The infiltration of PrP^{Sc} into the body is suggested to initiate the dysregulation of calcium homeostasis and unfolded protein response followed by neuronal dysfunction and apoptosis.[8] In addition, infectious PrP^{Sc} has been reported to activate p38-mitogen-activated protein kinase (MAPK) and subsequent neurodegeneration.[9] However, a detailed mechanism of prion diseases has not yet been elucidated. Currently, a definite diagnosis of prion diseases still relies on the detection of PrP^{Sc} in the postmortem brain tissue.[10] Recently, real-time quaking-induced conversion (RT-QUIC) that detects PrP^{Sc}

from the cerebrospinal fluid, olfactory mucosa, or both of patients with clinically suspected prion diseases has been proposed as an ultrasensitive and specific *ante mortem* diagnostic method for prion diseases.[11-12] However, further clinical trials of multiple patients with prion diseases at an early stage may be necessary to establish RT-QUIC as a standard diagnostic method. One of the neuropathological features of prion disease is amyloid plaque deposition consisting of PrP^{Sc} in the brain. Accordingly, visualization of PrP^{Sc} deposits in the living human brain could facilitate monitoring of prion disease progression and its characterization. Noninvasive imaging techniques such as single photon emission computed tomography (SPECT) and positron emission tomography (PET) are considered useful for visualizing prion deposition in the brain. Because PrP^{Sc} has a high beta-sheet content similar to beta-amyloid (Aβ) plaques, which are a hallmark of Alzheimer's disease (AD),[13] imaging probes for Aβ have been used to visualize PrP^{Sc} in patients with prion diseases. However, a few samples and contradictory results including negative reports, have hampered their usefulness in clinical practice, which has not been confirmed.[14] Actually, [^{11}C]PIB and [^{11}C]BF-227, which are Aβ imaging agents could not visualize patients with GSS and CJD, respectively.[15-16] Recently, we developed several radioligands, including flavonoid- and quinacrine-related compounds, as new prion imaging probes.[17-18] Among them, [^{123}I]SC-OMe (Fig. 1), a styryl chromone

derivative, could be used to visualize the prion deposits of mouse-adapted bovine spongiform encephalopathy (mBSE)-infected mice using a small animal SPECT/CT imaging system.[17] However, it may be necessary to develop new imaging agents with improved brain distribution, binding affinity, or both for PrP^{Sc} to obtain clearer and PrP^{Sc}-specific images.

Iodinated benzofuran (IBF) derivatives have been reported to exhibit potent binding affinities for $A\beta_{1-40}$ aggregates with K_i values of 0.4-9.0 nM and moderate brain uptake (>1.1% injected dose [ID]) in normal mice.[19] Since PrP^{Sc} forms a β-sheet rich structure similarly to Aβ aggregates, we considered that IBF backbone could be used for the development of PrP^{Sc} imaging probes. The 5-hydroxy-2-(4-methyaminophenyl)benzofuran, another benzofuran derivatives with lower lipophilicity, displayed high binding affinity for Aβ aggregates (K_i= 0.7 nM), excellent brain penetration (4.8%ID/g at 2 min after injection in mice), and rapid washout from normal brains (0.2%ID/g at 60 min).[20] Furthermore, 6-IBF derivatives exhibited a higher binding affinity for $A\beta_{1-40}$ aggregates than 5-IBF derivatives.[19] Therefore, the lipophilicity and position of iodine atoms may be important factors in the binding affinity to amyloid and brain distribution of these derivatives. Thus, we designed IBF derivatives with several substituents, including amino groups and an ethyleneoxy group, in the 4′-position and

attached an iodine atom to the 5 or 6 position of benzofuran derivatives as shown in Figure 2. We recently reported that rMoPrP aggregates and mBSE-infected mouse brain sections could be used to quantitatively evaluate PrP^{Sc} imaging agents.[17-18] Here, we describe the synthesis and evaluation of a series of IBF derivatives as prion imaging probes using these experimental tools.

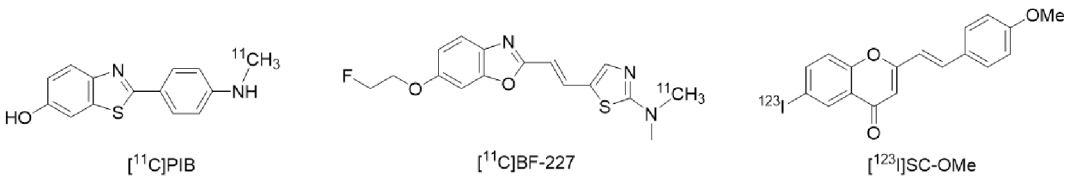

Figure 1. Chemical structures of reported imaging probes for visualization of scrapie prion protein (PrP^{Sc}).

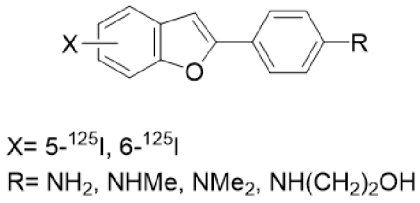

Figure 2. Chemical structures of iodobenzofuran (IBF) derivatives evaluated as scrapie prion protein (PrP^{Sc}) imaging probes in this study.

RESULTS AND DISCUSSION

Chemistry. The IBF derivatives were prepared as shown in scheme 1. Nucleophilic substitution of 4-nitrobenzyl bromide with 5-bromosalicylaldehyde or 4-bromosalicylaldehyde, followed by dehydration condensation to an aldehyde group formed phenyl benzofuran **1a** and **1b** with a yield of 79% and 39%, respectively. Each nitro group of **1a** and **1b** was reduced using tin chloride ($SnCl_2$) to obtain **2a** and **2b** with a yield of 20% and 69%, respectively. Treatment of **2a** and **2b** with tributyltin hydride [$(SnBu_3)_2$] and tetrakis(triphenylphosphine)palladium(0) [$(PPh_3)_4Pd$] generated the tributyltin derivative **3a** and **3b** (27% and 28% yield, respectively). Monomethylation of the aniline group of **2a** and **2b** with paraformaldehyde, sodium methoxide (NaOMe), and sodium tetrahydridoborate ($NaBH_4$) produced **4a** and **4b** at 90 and 85% yields, respectively. Compounds **2a** and **2b** were converted to the dimethyl derivatives **6a** and **6b** using paraformaldehyde, sodium cyanoborohydride, and acetic acid (74% and 74% yield, respectively). The tributyltin derivatives **5a**, **5b**, **7a**, and **7b** were prepared using a method similar to the one used to produce **3a** with yields of 39%, 39%, 55%, and 55%, respectively. The target IBF derivatives 5-IBF-NH_2, 6-IBF-NH_2, 5-IBF-NHMe, 6-IBF-NHMe, 5-IBF-NMe_2, and 6-IBF-NMe_2 were synthesized from the corresponding tributyltin derivatives at yields of 63%, 63%, 59%, 35%, 47%, and 39%, respectively. The 5-IBF-NHEtOH was synthesized as shown in scheme 2. Compound **2a** was alkylated

with 2-bromoethoxy-*tert*-butyl-dimethylsilane to produced **8** (40% yield), which was tributylstannylated to form compound **9** at a yield of 43%. The iodine derivative **10** was obtained by iodo-destannylation (28% yield), and deprotection of the *tert*-butyldimethylsilyl (TBS) group of **10** with tetrabutylammonium fluoride (TBAF) provided the target 5-IBF-NHEtOH at a yield of 17%. Radioiodination of the 5-IBF and 6-IBF derivatives was achieved using an iododestannylation reaction with hydrogen peroxide as an oxidant, which produced the desired radioiodinated ligands at yields of 20–70%, as shown in Scheme 3.

Scheme 1. Synthesis of iodobenzofuran (IBF) derivatives.

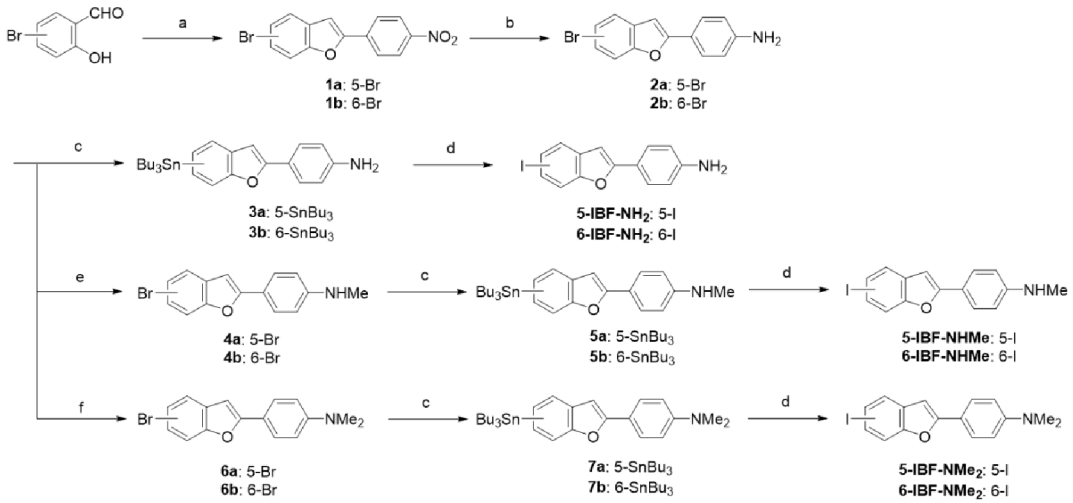

Reagents and conditions: (a) 4-nitrobenzyl bromide, K_2CO_3, DMF, 80 °C, 6-8 h; (b) $SnCl_2$, EtOH, reflux, 3-4 h; (c) $(SnBu_3)_2$, $(PPh_3)_4Pd$, TEA, dioxane, reflux, 6-7 h, (d) 1) I_2, $CHCl_3$, r.t., 10 min; 2) KF, $NaHSO_3$, rt; (e) 1) $(CHO)_n$, NaOMe, MeOH, 1h, 2) $NaBH_4$, reflux, 1 h; (f) $(CHO)_n$, $NaCNBH_3$, AcOH, rt, 3 h.

Scheme 2. Synthesis of 5-Iodo-2-(4-(2-ethanolamino)phenyl)benzofuran (5-IBF-NHEtOH).

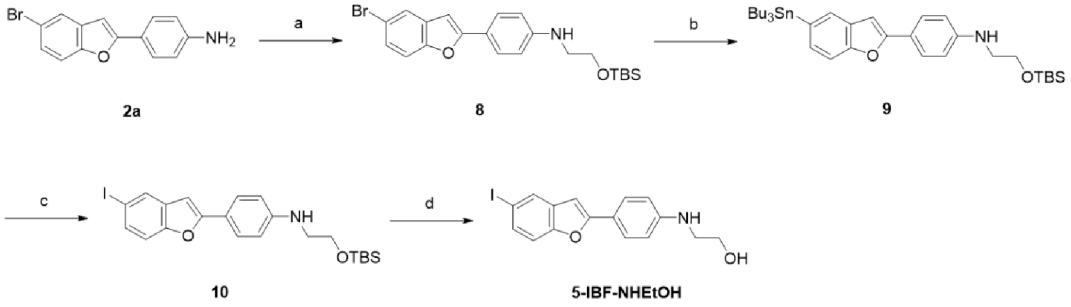

Reagents and conditions: (a) (2-bromoethoxy)-tert-butyldimethylsilane, K_2CO_3, DMF, 90 °C, 7 h; (b) $(SnBu_3)_2$, $(PPh_3)_4Pd$, TEA, dioxane, reflux, 6 h, (c) 1) I_2, $CHCl_3$, rt; 2) KF, $NaHSO_3$, rt, 10 min; (d) TBAF, THF, rt, 1 h.

Scheme 3. Radiosynthesis of ^{125}I-IBF derivatives.

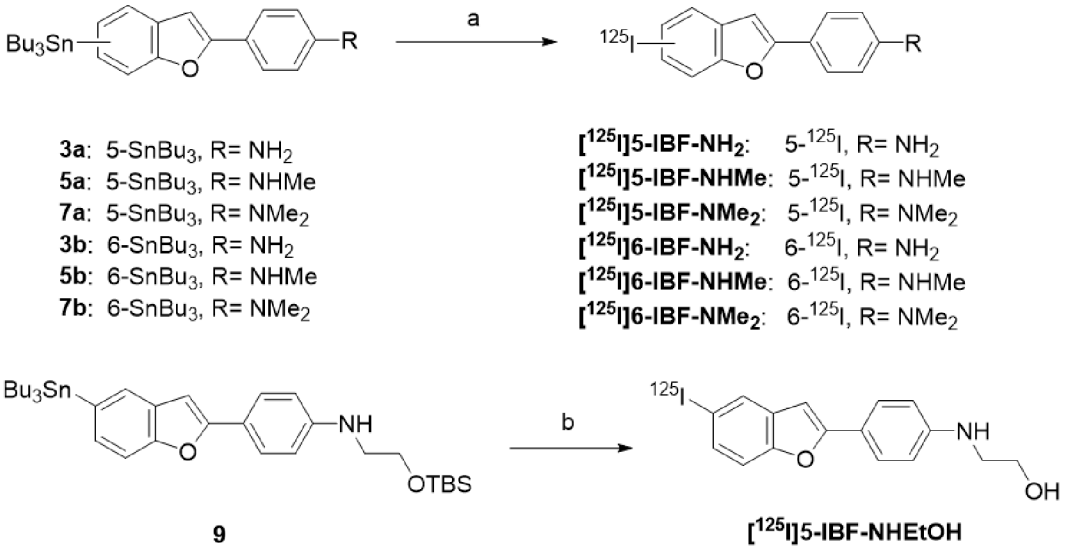

Reagents and conditions: (a) [^{125}I]NaI, H_2O_2, HCl, EtOH, rt, 10 min; (b) [^{125}I]NaI, H_2O_2, HCl, EtOH, rt, 20 min.

***In vitro* binding of IBF derivatives to rMoPrP aggregates.** In our previous studies, we used rMoPrP aggregates as PrP^{Sc} models to screen useful prion imaging probes.[17-18] Therefore, we evaluated the *in vitro* binding properties of the IBF derivatives to rMoPrP aggregates. First, we examined the radioactivities of the ^{125}I-IBF derivatives adsorbed on rMoPrP aggregates (0–500 nM) as shown in Figure 3. The adsorption rate of the ^{125}I-IBF

derivatives increased in a concentration-dependent manner to the rMoPrP aggregates and the bound ^{125}I-compound to 500 nM of aggregates ranged from 19.9 to 40.5%, indicating that all of the IBF derivatives showed potent absorptivity to rMoPrP aggregates. The adsorption rates of [^{125}I]5-IBF derivatives tended to be higher than those of [^{125}I]6-IBF derivatives. Since [^{125}I]5-IBF-NHMe exhibited the highest binding rate for rMoPrP aggregates, we further characterized the binding of [^{125}I]5-IBF-NHMe to rMoPrP aggregates using a saturation binding assay (Fig. 4). The binding of [^{125}I]5-IBF-NHMe to rMoPrP aggregates showed a saturated binding curve and linear Scatchard plot that fitted the single-binding site model. The equilibrium dissociation constant (K_d) of [^{125}I]5-IBF-NHMe was higher than that of [^{125}I]SC-NMe_2, which exhibited high affinity to PrP^{Sc} in the previous study[17] (K_d = 12.3 nM and 36.7 nM, respectively). Next, the inhibition constant (K_i) values of non-radioactive IBF derivatives for rMoPrP aggregates and $A\beta_{1-42}$ were evaluated using displacement studies of [^{125}I]5-IBF-NHMe. As shown in Table 1, the [^{125}I]5-IBF derivatives exhibited high affinities for rMoPrP aggregates in the order of [^{125}I]5-IBF-NHMe (K_i = 12.1 nM) > [^{125}I]5-IBF-NHEtOH (Ki = 34.1 nM) > [^{125}I]5-IBF-NMe_2 (K_i = 47.0 nM) > [^{125}I]5-IBF-NH_2 (K_i = 58.6 nM). The K_i values of [^{125}I]6-IBF ranged from 100 to 167 nM, which indicated that the introduction of an iodine atom in the 6 position diminished the binding interaction with rMoPrP aggregates. Both the

adsorption and inhibitory binding assays showed similar tendencies in the rank order of binding affinities. These results indicated that 2-ethanolamino at the 4′-position could maintain the binding affinity, but the most suitable substituent was *N*-monomethyl amino group for binding interaction with rMoPrP aggregates. In addition, it is thought that the introduction of iodine at the 5 rather than 6 position of IBF derivatives is advantageous for the binding affinity to rMoPrP rather. For $A\beta_{1-42}$ aggregates, all IBF derivatives exhibited strong binding affinities, which ranged from 0.51 to 21.8 nM of K_i values. It is reported that the binding affinities of 6-IBF derivatives for $A\beta_{1-40}$ aggregates are stronger than those of 5-IBF derivatives.[19] On the other hand, our study demonstrated that 5-IBF derivatives have slightly higher affinities than those of 6-IBF derivatives for $A\beta_{1-42}$ aggregates. It is unclear why these differences occur in the binding affinities of IBF derivatives among $A\beta_{1-40}$, $A\beta_{1-42}$ and rMoPrP. However, 5-IBF derivatives are possibly preferable PrP^{Sc} and $A\beta_{1-42}$ imaging probes, whereas 6-IBF derivatives could preferably serve as $A\beta_{1-40}$ imaging probes.

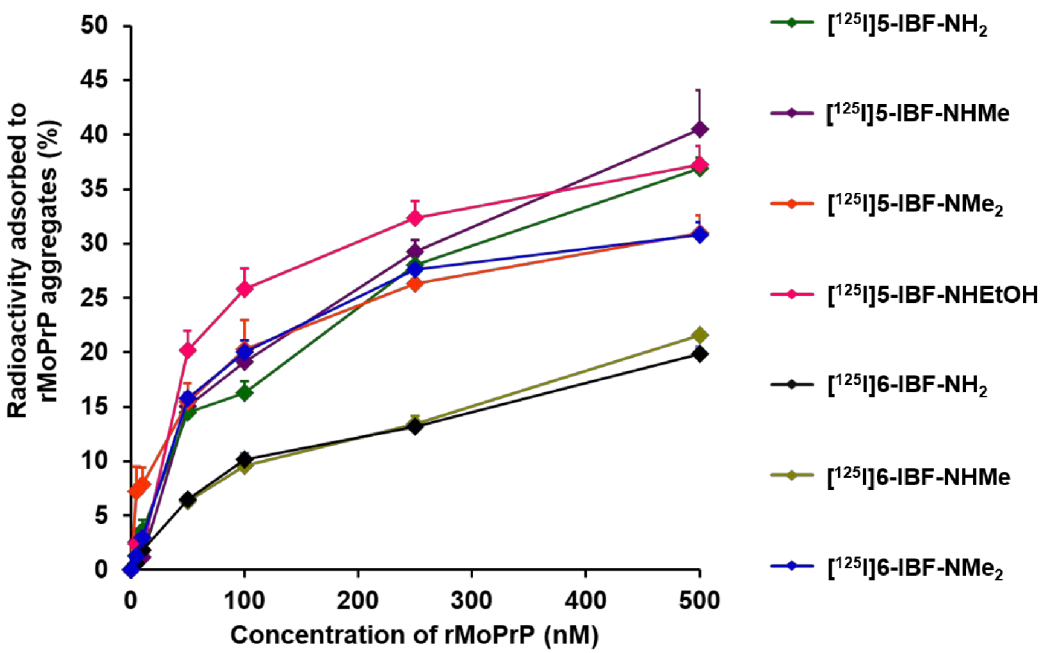

Figure 3. Radioactivity of ^{125}I-iodinated benzofuran (IBF) derivatives adsorbed to recombinant mouse prion protein (rMoPrP, 5.0–500 nM). Values are means ± standard error of the mean (SEM) of three independent measurements.

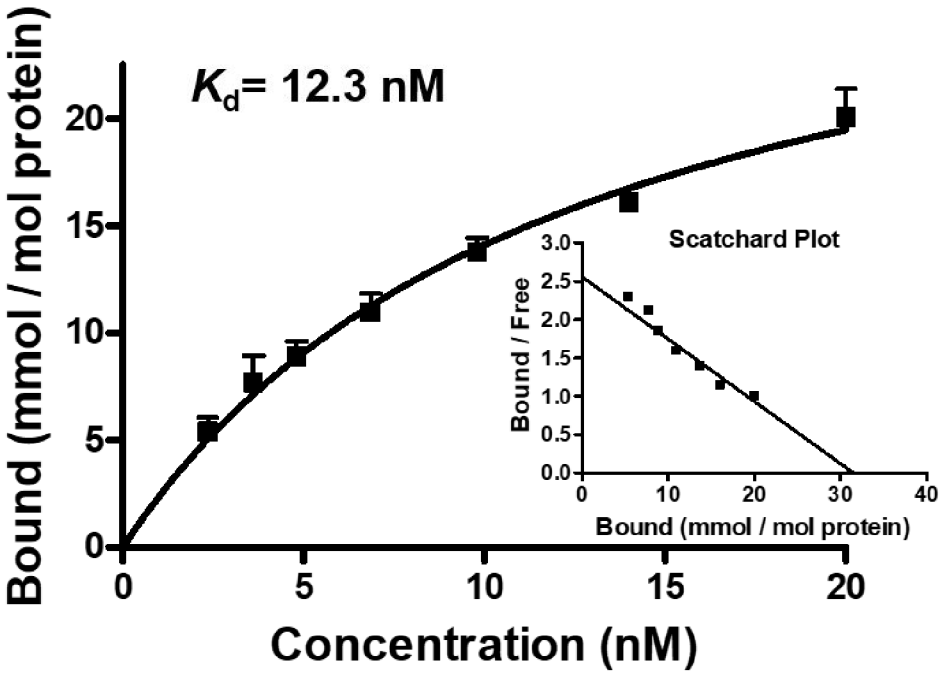

Figure 4. Saturation curve and Scatchard plot of [^{125}I]5-IBF-NHMe bound to recombinant mouse prion protein (rMoPrP) aggregates. Equilibrium dissociation constant (K_d) value was determined using saturation assays with increasing concentrations of 5-IBF-NHMe (2.4–20 nM).

Table 1. The K_i values of IBF derivatives for the binding of [^{125}I]5-IBF-NHMe to rMoPrP and $A\beta_{1-42}$ aggregates.

Compound	K_i (nM)[a]	
	rMoPrP	$A\beta_{1-42}$
5-IBF derivatives		
5-IBF-NH_2	58.6 (13.6)	11.8 (1.70)
5-IBF-NHMe	12.1 (1.90)	3.79 (0.15)
5-IBF-NMe_2	47.0 (14.5)	0.51 (0.02)
5-IBF-NHEtOH	34.1 (3.74)	3.14 (1.26)
6-IBF derivatives		
6-IBF-NH_2	112 (7.43)	21.8 (2.09)
6-IBF-NHMe	100 (14.0)	8.90 (0.51)
6-IBF-NMe_2	167 (3.09)	4.78 (0.34)

[a] Data represent the mean ± standard error of the mean for three independent experiments.

Fluorescence staining of 5-IBF derivatives in mBSE-infected mouse brain sections. Next, we evaluated the neuropathological fluorescence staining of 5-IBF derivatives in the brain sections isolated from mBSE-infected and mock-infected mice. Thioflavin T (ThT) was used for the identification of amyloid aggregates of PrP^{Sc} in the mouse brain sections similar to our previous studies.[18] As shown in Figure 5, each of the four 5-IBF derivatives (5-IBF-NH_2, 5-IBF-NHMe, 5-IBF-NMe_2, and 5-IBF-NHEtOH) showed clear fluorescence signals (Fig. 5A–D) at the ThT-labeled regions (Fig. 5E–H) in the corpus callosum region of mBSE-infected mouse brain sections. Regarding 5-IBF-NHMe, immunohistochemical analysis of PrP^{Sc} was further performed to confirm the binding site of 5-IBF-NHMe as a PrP^{Sc}-composed amyloid. As shown in Figure 6, fluorescence spots of 5-IBF-NHMe in the brain sections of mBSE-infected mice (Fig. 6A) corresponded to PrP^{Sc} deposit regions (Fig. 6B).

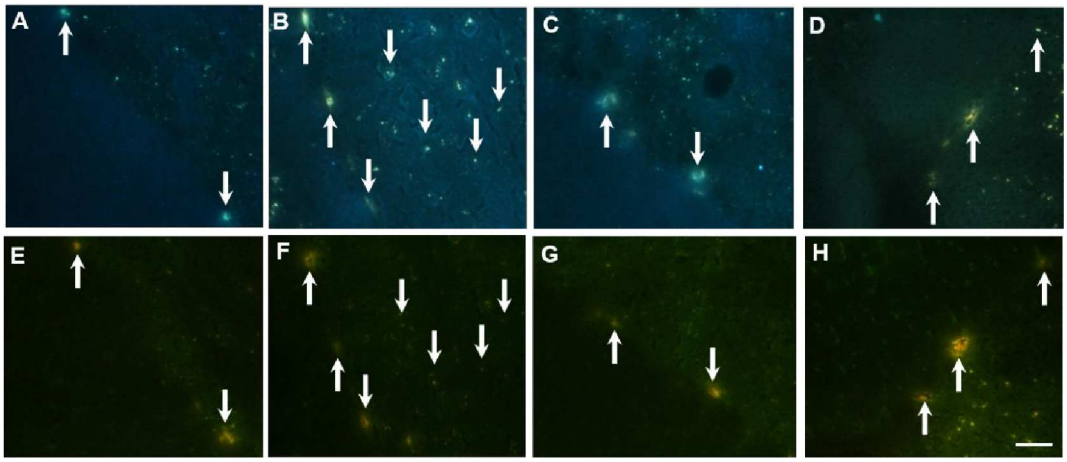

Figure 5. Fluorescence staining of 5-iodinated benzofuran (IBF) derivatives (5-IBF-NH_2, 5-IBF-NHMe, 5-IBF-NMe_2, and 5-IBF-NHEtOH) in brain sections of mouse-adapted bovine spongiform encephalopathy (mBSE)-infected mice (A–D). Scrapie prion protein (PrP^{Sc}) plaques were confirmed using Th-T (E–H). Scale bar = 20 μ m.

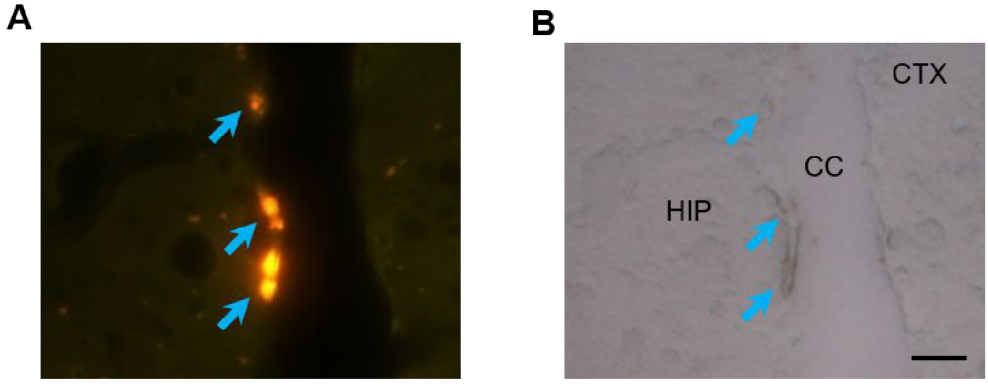

Figure 6. Fluorescence staining of 5-iodinated benzofuran (IBF)-NHMe in brain sections from mouse-adapted bovine spongiform encephalopathy (mBSE)-infected mice (A). Labeled amyloid deposits of (PrP^{Sc}) were confirmed by immunohistochemically staining each section using an anti-PrP antibody (B). Scale bar = 20 μ m. CTX; cerebral cortex, CC; corpus callosum, HIP; hippocampus.

***In vitro* autoradiography of [^{125}I]5-IBF-NHMe in mBSE- and mock-infected mouse brain sections.** To characterize [^{125}I]5-IBF-NHMe as a prion imaging probe, further *in vitro* autoradiography studies were performed in mBSE- and mock-infected mouse brain sections. [^{125}I]5-IBF-NHMe exhibited high signals in the right corpus callosum region of mBSE-infected mice (Fig. 7A), which spatially matched the distribution of PrP^{Sc} deposits (Fig. 7D). In contrast, these tracers showed no significant

accumulation in the contralateral side of the brain (Fig. 7A), which showed no significant PrP^{Sc} deposits (Fig. 7C). We observed that the tracer exhibited an almost homogeneous distribution of radioactivity in the brain sections of mock-infected mice (Fig. 7B) without significant evidence of PrP^{Sc} deposits (Fig. 7E and F). These results confirmed that [^{125}I]5-IBF-NHMe was highly and specifically bound to the cerebral PrP^{Sc} deposits.

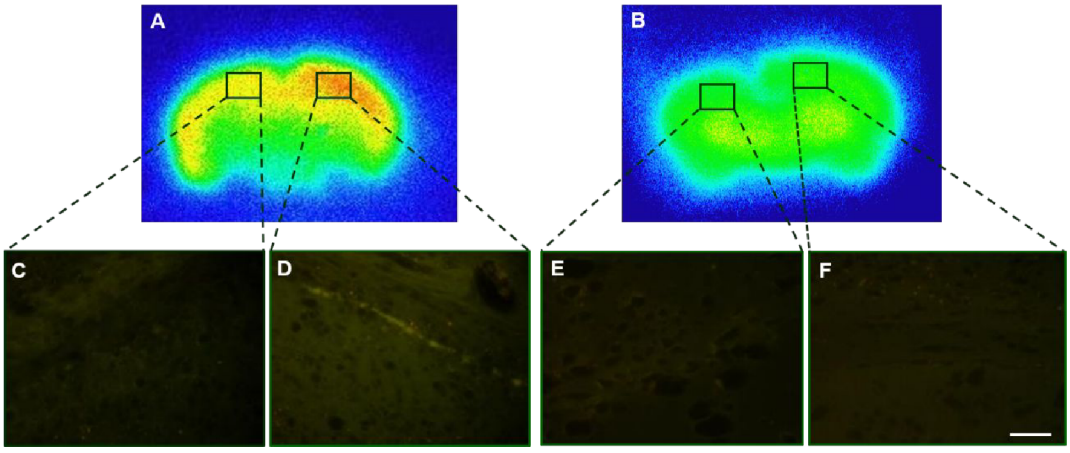

Figure 7. *In vitro* autoradiograms of the mBSE-infected (A) and mock-infected (B) mice brain labeled with [^{125}I]5-IBF-NHMe. Scrapie prion protein (PrP^{Sc}) plaques were confirmed using ThS (C–F). Scale bar= 50 μ m.

***In vivo* biodistribution in normal mice.** Clinically available *in vivo* imaging probes for amyloid are expected to show good brain penetration and low nonspecific binding to the off-target regions in the brain.[21] In a previous study, the *in vivo* biodistribution studies of several ^{125}I-IBF derivatives ([^{125}I]5-IBF-NHMe, [^{125}I]5-IBF-NMe_2, and [^{125}I]6-IBF-NMe_2) were reported.[19] These tracers showed moderate initial brain uptake but slow clearance from the normal brain. Although IBF derivatives, especially 5-IBF-NHMe showed prospective binding affinity to PrP^{Sc} deposits *in vitro*, [^{125}I]5-IBF-NHMe may not be a suitable *in vivo* tracer for visualization of PrP^{Sc}. Therefore, we performed biodistribution studies of ^{125}I-labeled 5-IBF and 6-IBF derivatives, including the newly developed compounds (5-IBF-NH_2, 5-IBF-NHEtOH, 6-IBF-NH_2, and 6-IBF-NHMe) to identify scaffolds of useful *in vivo* imaging probes with an IBF backbone. We did not evaluate the *in vivo* biodistribution of [^{125}I]6-IBF-NMe_2 because this compound has already been demonstrated to show quite poor blood-brain-barrier (BBB) permeability.[19] As shown in Figures 8 and 9, the brain distribution and peripheral region data were expressed as the percentage injected dose per gram (%ID/g), respectively. The brain uptake of IBF derivatives tended to improve with decreasing lipophilicity. Specifically, [^{125}I]6-IBF-NH_2 showed the highest peak brain uptake (2.59% ID/g, 10 min) and good clearance (0.51% ID/g, 180 min). [^{125}I]5-IBF-NHEtOH showed

greater brain uptake than any of the other 5-IBF derivatives did, but considerable radioactivity was still retained in the brain 180 min after the injection (1.72 ID/g). Both 5-IBF and 6-IBF derivatives showed high uptake into the lungs and peaked at 2 min in the following order of increasing magnitude: NMe_2 forms > NHMe forms > NH_2 forms. The brain uptake of these IBF derivatives increased gradually after administration and reached the maximum value after 10 to 60 minutes, which may have been due to delayed brain inflow from peripheral tissues. In fact, the pulmonary radioactivity gradually decreased, which may be one of the reasons for the delayed brain accumulation of IBF derivatives. The uptake of these [^{125}I]IBF derivatives in the thyroid gland gradually increased and reached 28.0–199% dose/g 180 min after the injection (Fig. 9), indicating that these radioligands were deiodinated *in vivo*. Since the brain uptake decreased after 60 min, it seemed unlikely that the metabolites accumulated in the brain. Radiotracers with a low molecular weight (MW) (< 500 Da) and moderate lipophilicity {log P (partition coefficient) values, 2.0–3.5} have been reported to show optimal passive brain entry *in vivo*.[22-23] The molecular weights of these IBF derivatives were within 500 Da, but their calculated log P values were higher than the optimal range. In this study, we observed three IBF derivatives, [^{125}I]5-IBF-NH_2, [^{125}I]5-IBF-NHEtOH, and [^{125}I]6-IBF-NH_2, with suitable lipophilicity for BBB permeability with Clog P values of 3.93, 3.72,

and 3.93, respectively (Table 2), which showed preferable brain uptake compared with that of other more lipophilic IBF derivatives. We observed that the clearance of the new ^{125}I-IBF derivatives from brain was still slow, indicating that these compounds may have other off-target binding sites in the brain as suggested in a previous study of IBF derivatives.[19] Recently, a central nervous system multiparameter PET optimization (CNS PET MPO) algorithm has been built to predict the favorable physicochemical properties of clinically useful CNS PET tracers.[24,25] Therefore, we also calculated the ClogD (calculated distribution coefficient at pH = 7.4), HBD (number of hydrogen bond donors), and pKa (ionization constant of the most basic center) as shown in Table 2. Zhang et al. proposed that desirable ranges were defined as ClogP ≤ 2.8, ClogD ≤ 1.7, MW ≤ 305.3, 44.8 < TPSA ≤ 63.3, HBD ≤ 1, and pKa ≤ 7.2. They set the desirability scores of each parameter ranging from 0.0 to 1.0 and CNS PET MPO scores >3 have been shown to increase the overall probability of success for CNS PET ligand development in their database.[24] Although the CNS PET MPO scores of all seven IBF derivatives in this study were below 3, it is demonstrated that the 5-IBF-NH_2 and 6-IBF-NH_2 with the highest CNS PET MPO values (2.6) have relatively high BBB permeability. As an exception, the CNS PET MPO of [^{125}I]5-IBF-NHEtOH that showed the highest brain uptake among 5-IBF derivatives was 2.0. In our previous study, a ^{11}C-labeled benzofuran derivative in which

the iodine atom of [^{125}I]5-IBF-NHMe was substituted with a hydroxyl group showed high brain penetration and rapid disappearance from the brain tissue.[20] In addition, two ^{18}F-labeled benzofuran derivatives with a pyridyl group ([^{18}F]FPYBF-2 and [^{18}F]FPHBF-2) have been reported to show high brain penetration and good clearance properties.[26] Considering that the CNS PET MPO scores of these three PET radioligands were calculated to range from 3.7 to 4.0, this algorithm may be a strong predictor for the development of new benzofuran derivatives as amyloid imaging probes. Taken together, further reduction in lipophilicity and/or molecular weight with minimum hydrogen bond donors of IBF derivatives due to the introduction of various hydrophilic substituent groups without hydrogen donors and large substituents could improve the initial brain uptake and rapid clearance with reduced non-specific binding to off-target regions. On the other hand, the basic structure of IBF derivatives is similar to that of PIB and BF227. Therefore, it should be taken in consideration that IBF derivatives recognize the β-sheet structure in amyloid fibrils and can bind to both PrP^{Sc} and Aβ deposits in the living brain. In fact, we observed that IBF derivatives have high binding affinities to both Aβ and rMoPrP aggregates in this study. It is reported that PrP deposition was detected in the cerebral neocortex of sCJD patients.[27] In GSS patients, numerous PrP plaques were detected not only in the cerebrum but also in the cerebellum, and PrP^{Sc} and Aβ deposit

were simultaneously present in the cerebral cortex.[28] The appearance of Aβ deposits in the neocortex originated from the early phase, but deposits in the cerebellum were detected only in the end phase of AD patients.[29] Therefore, detection of amyloid plaques in the cerebellum by non-selective amyloid imaging probes may facilitate distinction of GSS from other amyloid diseases in some cases. However, it is considered desirable to use amyloid selective imaging probes to accurately distinguish between CJD and AD. Since the IBF derivatives exhibited excellent binding affinity and could detect PrP^{Sc} deposits in the brain tissues, optimization of PrP^{Sc} selectivity and CNS PET MPO scores of IBF derivatives could be potentially useful *in vivo* imaging probes for PrP^{Sc}.

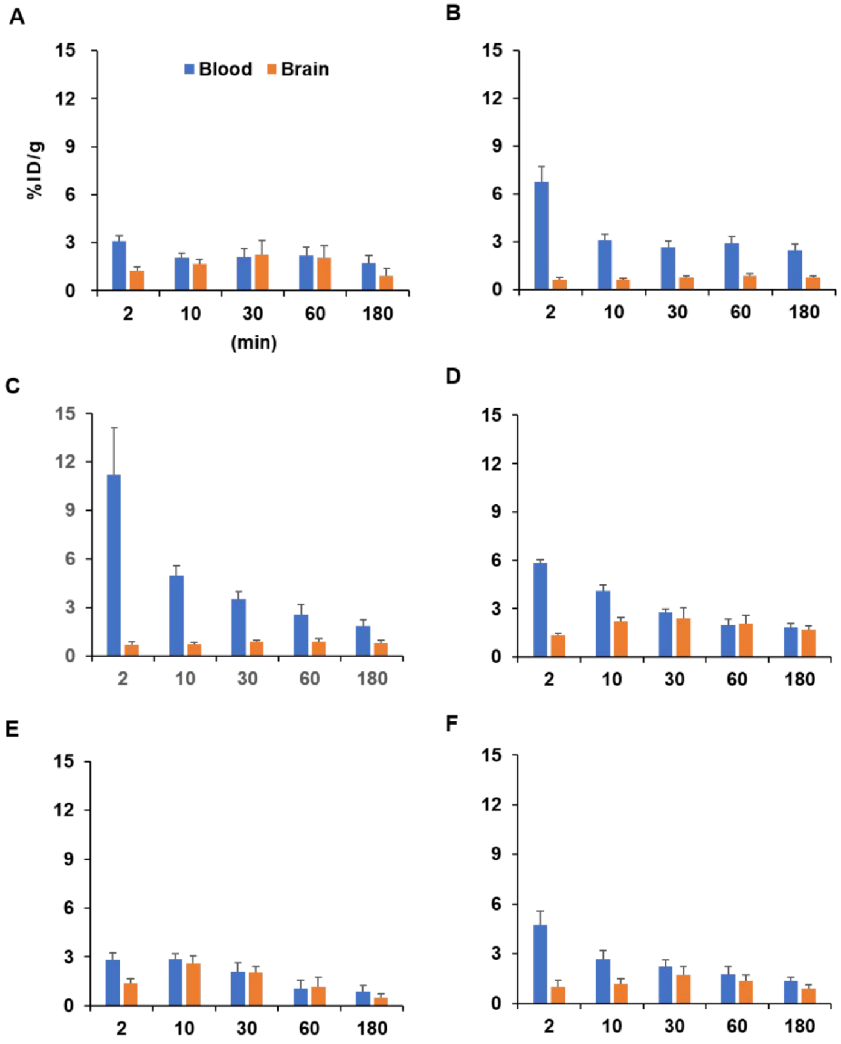

Figure 8. Blood and brain distribution of the radioactivity after intravenous administration of [^{125}I]5-IBF-NH_2 (A), [^{125}I]5-IBF-NHMe (B), [^{125}I]5-IBF-NMe_2 (C), [^{125}I]5-IBF-NHEtOH (D), [^{125}I]6-IBF-NH_2 (E), [^{125}I]6-IBF-NHMe (F) and [^{125}I]6-IBF-NMe_2 (G) in mice. Data are expressed as percent injected dose per gram (%ID/g). Each value represents the mean (standard deviation) of 5–7 mice.

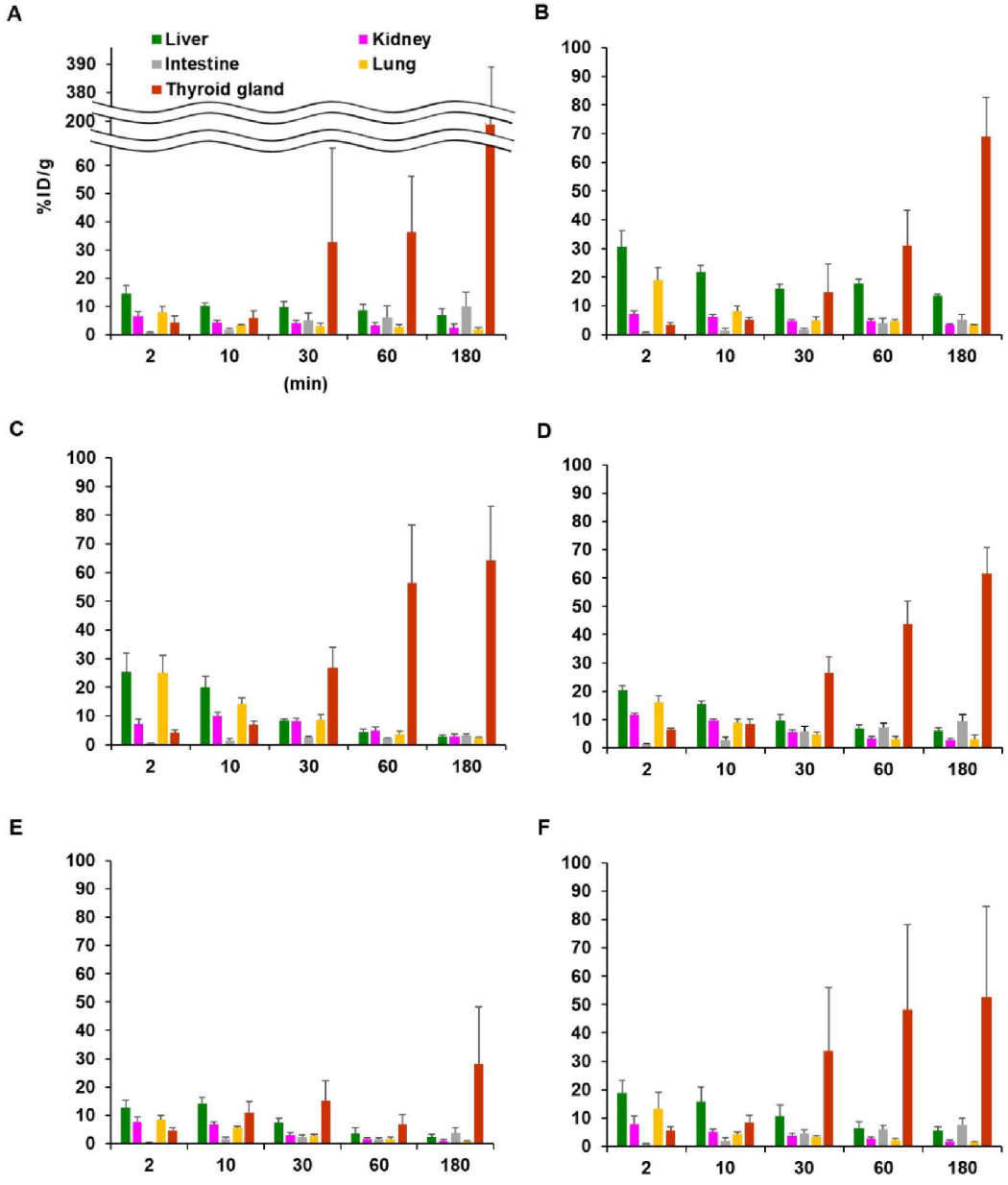

Figure 9. Biodistribution of the radioactivity after intravenous administration of [^{125}I]5-IBF-NH_2 (A), [^{125}I]5-IBF-NHMe (B), [^{125}I]5-IBF-NMe_2 (C), [^{125}I]5-IBF-NHEtOH (D), [^{125}I]6-IBF-NH_2 (E), [^{125}I]6-IBF-NHMe (F) and [^{125}I]6-IBF-NMe_2 (G) in the peripheral

organs of mice. Data are expressed as percent injected dose per gram (%ID/g). Each value represents the mean (standard deviation) of 5–7 mice.

Table 2. Individual CNS PET MPO parameters of ^{125}I-IBF derivatives.

Compound	ClogP[a]	ClogD[b]	TPSA[a]	Mw	HBD	pKa[b]	CNS PET MPO[c]
5-IBF-NH_2	3.93	4.57	35.25	335.14	1	3.52	2.6
5-IBF-NHMe	4.23	5.02	21.26	349.17	1	3.88	2.0
5-IBF-NMe_2	5.02	5.42	12.47	363.2	1	4.27	2.0
5-IBF-NHEtOH	3.72	4.73	41.49	379.2	2	3.48	2.0
6-IBF-NH_2	3.93	4.56	35.25	335.14	1	3.52	2.6
6-IBF-NHMe	4.23	5.01	21.26	349.17	1	3.87	2.0
6-IBF-NMe_2	5.02	5.41	12.47	363.2	1	4.27	2.0

[a] The physicochemical properties of each compound was calculated using a ChemBioDraw Ultra 13.0.

[b] The physicochemical properties of each compound was calculated using a SPARK on line calculator.

[c] The CNS PET MPO of each compound was calculated according to the literature. [24]

ClogP, calculated partition coefficient; ClogD, calculated distribution coefficient at pH=7.4; MW, molecular weight; TPSA, topological polar surface area; HBD, number of hydrogen bond donors, pKa, ionization constant of the most basic center.

CONCLUSION

We synthesized and evaluated a series of 5-IBF and 6-IBF derivatives as prion imaging probes. All the IBF derivatives investigated exhibited potent adsorption to rMoPrP aggregates, especially [^{125}I]5-IBF-NHMe, which had an excellent binding affinity with a K_d value of 12.3 nM. Fluorescence imaging and autoradiography studies of 5-IBF-NHMe showed clear signals at the PrP^{Sc}-positive amyloid deposits in the mBSE-infected mouse brain model. Although further structure-activity relationship studies should be done to optimize the *in vivo* brain distribution, IBF derivatives have prospective properties as prion imaging probes.

EXPERIMENTAL SECTION

Materials. All reagents were commercial products and were used without further purification, unless otherwise indicated. [^{125}I]NaI was purchased from Muromachi Yakuhin (Tokyo, Japan). The ^{1}H NMR spectra were obtained using a Varian Gemini 300 spectrometer or a JEOL JNM-AL 400 spectrometer with tetramethylsilane (TMS) as an internal standard. The mass spectra were obtained using JMS-T100TD or JMS-700N mass spectrometer (JEOL, Japan). High-performance liquid chromatography (HPLC) analysis and purification were performed using a Shimadzu HPLC system (LC-10AT pump with SPD-10A UV detector, λ = 254 nm). An automated gamma counter with a NaI(Tl) detector (2470 WIZARD^{2}, PerkinElmer, MA, USA) was used to measure the radioactivity. The experiments with animals were conducted in accordance with our institutional guidelines and were approved by Nagasaki University Animal Care Committee.

Chemistry.

*5-Bromo-2-(4-nitrophenyl)benzofuran (**1a**)*. A mixture of 5-bromosalicylaldehyde (3.0 g, 15.0 mmol) and K_2CO_3 in DMF (20 mL) was added 4-nitrobenzyl bromide (3.24 mg, 15.00 mmol) and heated at 80 °C for 6 h. After the mixture cooled to room

temperature, the reaction mixture was filtrated and washed with water. The residue was collected and dried by vacuum pump to give **1a** (3.76 g, 79%) as a yellow solid. ^{1}H NMR (300MHz, $CDCl_3$) δ 7.18 (s, 1H), 7.46-7.45 (m, 2H), 7.78 (d, *J*= 0.6 Hz, 1H), 8.00 (d, *J*= 9.0 Hz, 2H), 8.33 (d, *J* = 9.0 Hz, 2H). MS (DART) *m/z* 319 $[M+H]^+$

*6-Bromo-2-(4-nitrophenyl)benzofuran (**1b**)*. The procedure used for preparation of **1a** was employed to obtain compound **1b** (614 mg, 39%) from 4-bromosalicylaldehyde (1.0 g, 5.0 mmol). ^{1}H NMR (300MHz, $CDCl_3$) δ 7.20 (s, 1H), 7.41 (dd, *J*= 8.0 Hz, 1.6 Hz, 1H), 7.51 (d, *J*= 8.4 Hz, 1H), 7.74 (s, 1H), 7.99 (d, *J*= 8.0 Hz, 2H), 8.32 (d, *J*= 8.0 Hz, 2H). MS (DART) *m/z* 316 $[M+H]^+$.

*5-Bromo-2-(4-aminophenyl)benzofuran (**2a**)*. A mixture of **1a** (2.0 g, 6.31 mmol), $SnCl_2$ (5.98 g, 31.6 mmol), and ethanol (20 mL) was stirred under reflux for 3 h. After the mixture cooled to room temperature, 1 M NaOH (20 mL) was added and extracted with ethyl acetate. The combined organic layers were dried with Na_2SO_4 and evaporated to dryness. The crude product was subjected to chromatographic purification on silica gel using EtOAc/hexane/Et_3N (50:50:1) to give **2a** (360 mg, 20%) as a pale yellow solid. ^{1}H NMR (300MHz, $CDCl_3$) δ 3.84 (bs, 2H), 6.75 (d, *J*= 8.4 Hz, 2H), 7.21 (s, 1H), 7.30 (dd,

J= 8.1, 1.2 Hz, 1H), 7.34 (d, *J*= 8.2 Hz, 2H), 7.65 (d, *J*= 8.7 Hz, 2H). MS (DART) *m/z* 289 $[M+H]^+$.

*6-Bromo-2-(4-aminophenyl)benzofuran (**2b**).* A mixture of **1b** (500 mg, 1.58 mmol) and 10% Pd/C (31.5 mg) in EtOAc was vigorously stirred under hydrogen atmosphere at room temperature for 13.5 h. The crude product was subjected to chromatographic purification on silica gel using EtOAc/hexane (1: 3) to give **2b** (312 mg, 69%). ^{1}H NMR (400MHz, $CDCl_3$) δ 3.87 (br, 2H), 6.73 (s, 1H), 6.75 (s, 1H), 6.76 (s, 1H), 7.30 (m, 2H), 7.63 (s, 2H), 7.65 (s, 1H). MS (DART) *m/z* 286 $[M+H]^+$.

*5-(Tributylstannyl)-2-(4-aminophenyl)benzofuran (**3a**).* A mixture of **2a** (300 mg, 1.05 mmol), $(Bu_3Sn)_2$ (2.64 mL, 5.23 mmol), and $(Ph_3P)_4Pd$ (242 mg, 0.21 mmol) in a solvent mixture (5 mL, 3:1 dioxane/Et_3N) was stirred under reflux for 6 h. The solvent was removed, and the residue was purified by silica gel chromatography using $CHCl_3$/hexane (1:4) to yield **3a** (141 mg, 27%) as a yellow oil. ^{1}H NMR (300MHz, $CDCl_3$) δ 0.89 (t, *J*= 7.2 Hz, 9H), 1.08 (dd, *J*= 8.4, 8.1 Hz, 6H), 1.34 (sext, *J*= 7.8 Hz, 6H), 1.55 (sext, *J*= 7.9 Hz, 6H), 3.79 (bs, 1H), 6.71 (d, *J*= 8.4 Hz, 2H), 6.78 (d, *J*= 0.9 Hz, 1H), 7.30 (dd, *J*=8.0, 0.9 Hz, 1H), 7.46 (d, *J*= 8.0 Hz, 1H), 7.61 (s, 1H), 7.66 (d, *J*=

8.4 Hz, 2H). MS (DART) *m/z* 500 $[M+H]^+$.

*6-(Tributylstannyl)-2-(4-aminophenyl)benzofuran(**3b**)*. The procedure used for preparation of **3a** was employed to obtain compound **3b** (12 mg, 28%) from **2b** (25 mg, 0.087 mmol). ^{1}H NMR (300MHz, $CDCl_3$) δ 0.86-0.91 (m, 9H), 1.06-1.11 (m, 6H), 1.30-1.38 (m, 6H), 1.51-1.59 (m, 6H), 3.81 (br, 2H), 6.73 (d, *J* = 8.7Hz, 2H), 6.79 (s,1H), 7.26 (d, *J* = 7.2Hz, 1H), 7.51 (d, *J* = 7.2Hz, 1H), 7.59 (s, 1H), 7.67 (d, *J* = 8.7Hz, 2H). MS (DART) *m/z* 500 $[M+H]^+$.

*5-Iodo-2-(4-aminophenyl)benzofuran (**5-IBF-NH$_2$**)*. A solution of iodine in $CHCl_3$ (1.0 mL, 1.0 M) was added to a solution of **3a** (50 mg, 0.1 mmol) in $CHCl_3$ (1.5 mL) at room temperature, and the mixture was stirred at room temperature for 10 min. A saturated $NaHSO_3$ solution (10 mL) was added, and then 1.0 M aqueous KF solution (10 mL) was added. organic layer was separated and the aqueous layer was extracted with $CHCl_3$. The combined organic layers were dried with Na_2SO_4 and evaporated to dryness. The crude product was subjected to chromatographic purification on silica gel using $CHCl_3$/hexane (2:3) to give 5-IBF-NH_2 (21 mg, 63%) as a white powder. ^{1}H NMR (300MHz, $CDCl_3$) δ 3.95 (bs, 2H), 6.74 (d, *J*= 8.4 Hz, 2H), 6.74 (s, 1H), 7.28-7.36 (m,

2H), 7.63 (s, 1H), 7.65 (d, *J*= 8.7 Hz, 2H). ^{13}C NMR (100MHz, $CDCl_3$) δ 157.7, 153.9, 147.3, 132.4, 129.0, 126.6, 124.4, 120.3, 115.0, 112.8, 97.5, 86.2 MS (DART) *m/z* 336 $[M+H]^+$.

*6-Iodo-2-(4-aminophenyl)benzofuran(**6-IBF-NH$_2$**)*. The procedure used for preparation of 5-IBF-NH_2 was employed to obtain 6-IBF-NH_2 (5.0 mg, 63%) from **3b** (12 mg, 0.02 mmol). ^{1}H NMR (400MHz, $CDCl_3$) δ 1.64 (br, 2 H), 6.74 (d, *J* = 8.8Hz, 2 H), 6.76 (s, 1 H), 7.27 (d, *J* = 8Hz, 1 H), 7.49 (d, *J* = 8Hz, 1 H), 7.64 (d, *J* = 6Hz, 2 H), 7.83 (s, 1 H). ^{13}C NMR (100MHz, $CDCl_3$) δ 157.7, 154.7, 146.5, 131.7, 129.4, 126.5, 121.6, 120.3, 120.0, 115.0, 98.3, 85.7 MS (DART) *m/z* 334 $[M+H]^+$.

*5-Bromo-2-(4-methylaminophenyl)benzofuran (**4a**)*. To a mixture of **2a** (381 mg, 1.33 mmol) and paraformaldehyde (199 mg, 6.64 mmol) in MeOH (15 mL) was added a solution of 28 wt % NaOMe in MeOH (0.35 mL, 1.99 mmol) dropwise at 0 °C. The mixture was stirred under reflux for 1 h. After addition of $NaBH_4$ (191 mg, 5.31 mmol), the solution was heated under reflux for 1 h. After the mixture cooled to room temperature, 1 M NaOH (30 mL) was added followed by extraction with CH_2Cl_2 (30 mL × 2). The combined organic layers were dried with Na_2SO_4 and evaporated to dryness. The crude

product was subjected to chromatographic purification on silica gel using EtOAc/hexane (1:3) to give **4a** (358 mg, 90%) as a yellowish brown powder. ^{1}H NMR (300MHz, $CDCl_3$) δ 2.90 (s, 3 H), 4.10 (bs, 1 H), 6.66 (d, *J*= 8.7 Hz, 2 H), 6.72 (d, *J*= 0.9 Hz, 1 H), 7.26-7.35 (m, 2 H), 7.62 (d, *J*= 1.5 Hz, 1 H), 7.68 (d, *J*= 9.0 Hz, 2 H). MS (DART) *m/z* 303 $[M+H]^+$.

*6-Bromo-2-(4-methylaminophenyl)benzofuran (**4b**)*. The procedure used for preparation of **4a** was employed to obtain **4b** (225 mg, 85%) from **2b** (252 mg, 0.88 mmol). ^{1}H NMR (300MHz, $CDCl_3$) δ 2.90 (s, 3 H), 4.03 (bs, 1 H), 6.66 (*J*= 9.0 Hz, 2 H), 6.74 (d, *J*= 1.2 Hz), 7.28 (d, *J*= 1.8 Hz), 7.31 (d, *J* = 1.5 Hz, 1 H), 7.35 (s, 1 H), 7.63 (s, 1 H), 7.67 (d, *J* = 9.0 Hz, 2 H). MS (DART) *m/z* 303 $[M+H]^+$.

*5-(Tributylstannyl)-2-(4-methylaminophenyl)benzofuran (**5a**)*. The procedure used for preparation of **3a** was employed to obtain compound **5a** (199 mg, 39%) from **4a** (300 mg, 1.00 mmol). ^{1}H NMR (300MHz, $CDCl_3$) δ 0.89 (t, *J*= 7.2 Hz, 9H), 1.07 (dd, *J*= 8.4, 8.1 Hz, 6H), 1.34 (sext, J= 7.8 Hz, 6H), 1.44-1.78 (m, 6H), 2.82 (s, 3H), 3.85 (bs, 1H), 6.62 (d, *J*= 9.0 Hz, 2H), 6.76 (d, *J*= 0.9 Hz, 1H), 7.27 (d, *J*= 8.1 Hz, 1H), 7.46 (d, *J*= 8.1 Hz, 1H), 7.61 (s, 1H), 7.68 (d, *J*= 8.7 Hz, 2H). MS (DART) *m/z* 513 $[M+H]^+$.

*6-(Tributylstannyl)-2-(4-methylaminophenyl)benzofuran (**5b**).* The procedure used for preparation of **3a** was employed to obtain **5b** (150 mg, 39%) from **4b** (225 mg, 0.88 mmol). ^{1}H NMR (300MHz, $CDCl_3$) δ 0.89 (t, *J*= 7.5 Hz, 9H), 1.02-1.42 (m, 12H), 1.44-1.78 (m, 6H), 2.88 (s, 3H), 3.90 (s, 1H), 6.65 (d, *J*= 8.7 Hz, 2H), 6.76 (d, *J*= 0.9 Hz, 1H), 7.25 (d, *J*= 7.2 Hz, 1H), 7.50 (d, *J*= 7.8 Hz, 1H), 7.59 (s, 1H), 7.70 (d, *J*= 9.0 Hz, 2H). MS (DART) *m/z* 513 $[M+H]^+$.

*5-Iodo-2-(4-methylaminophenyl)benzofuran (**5-IBF-NHMe**).* The procedure used for preparation of 5-IBF-NH_2 was employed to obtain 5-IBF-NHMe (40 mg, 59%) from **5a** (100 mg, 0.19 mmol). ^{1}H NMR (300MHz, $CDCl_3$) δ 2.90 (s, 3 H), 4.02 (bs, 1 H), 6.66 (d, *J*= 8.7 Hz, 2H), 6.70 (s, 1H), 7.24 (d, *J*= 8.2 Hz, 1H), 7.47 (dd, *J*= 8.1, 1.5 Hz, 1H), 7.67 (d, *J*= 8.7 Hz, 2H), 7.83 (d, *J*= 1.5 Hz, 1H). ^{13}C NMR (100MHz, $CDCl_3$) δ 158.0, 153.9, 149.9, 131.6, 128.9, 126.5, 123.1, 118.8, 112.7, 112.2, 97.0, 86.2, 30.5. MS (DART) *m/z* 350 $[M+H]^+$.

*6-Iodo-2-(4-methylaminophenyl)benzofuran(**6-IBF-NHMe**).* The procedure used for preparation of 5-IBF-NH_2 was employed to obtain 6-IBF-NHMe (24 mg, 35%) from **5b**

(100 mg, 0.20 mmol). ^{1}H NMR (300MHz, $CDCl_3$) δ 2.90 (s, 3H), 3.99 (bs, 1H), 6.65 (d, *J*= 8.7 Hz, 2H), 6.73 (s, 1H), 7.26 (d, *J*= 7.8 Hz, 1H), 7.48 (dd, *J*= 8.1, 1.5 Hz, 1H), 7.67 (d, *J*= 8.7 Hz, 2H), 7.82 (s, 1H). ^{13}C NMR (100MHz, $CDCl_3$) δ 157.4, 155.0, 149.9, 131.6, 129.5, 126.5, 121.5, 120.0, 118.9, 112.2, 97.8, 85.9, 30.5. MS (DART) *m/z* 350 $[M+H]^+$.

*5-Bromo-2-(4-dimethylaminophenyl)benzofuran (**6a**).* To a stirred mixture of **2a** (300 mg, 1.05 mmol) and paraformaldehyde (251 mg, 8.36 mmol) in AcOH (13 mL) was added $NaCNBH_3$ (328 mg, 5.23 mmol) in one portion at room temperature. The resulting mixture was stirred at room temperature for 3 h, and 1 M NaOH (50 mL) was added followed by extraction with EtOAc (25 × 2 mL). The combined organic layers were dried with Na_2SO_4 and evaporated to dryness. The crude product was subjected to chromatographic purification on silica gel using $CHCl_3$/hexane (2:3) to give **6a** (245 mg, 74%) as a yellowish brown powder. ^{1}H NMR (300MHz, $CDCl_3$) δ 3.03 (s, 6H), 6.72 (s, 1H), 6.76 (d, *J*= 8.7 Hz, 2H), 7.29 (d, *J* = 0.9 Hz, 1H), 7.32 (s, 1 H), 7.62 (d, *J* = 1.8 Hz, 1H), 7.71 (d, *J* = 8.7 Hz, 2H). MS (DART) *m/z* 317 $[M+H]^+$.

*6-Bromo-2-(4-dimethylaminophenyl)benzofuran (**6b**).* The procedure used for preparation of **6a** was employed to obtain **6b** (82 mg, 74%) from **2b** (100 mg, 0.35 mmol).

^{1}H NMR (300MHz, $CDCl_3$) δ 3.01 (s, 6H), 6.77 (*J*= 9.6 Hz, 2 H), 7.31 (dd, *J*= 8.7, 1.9 Hz, 1H), 7.37 (d, *J* = 8.0 Hz, 1H), 7.64 (s, 1H), 7.71 (d, *J* = 9.0 Hz, 2H). MS (DART) *m/z* 317 $[M+H]^+$.

*5-(Tributylstannyl)-2-(4-dimethylaminophenyl)benzofuran (**7a**)*. The procedure used for preparation of **3a** was employed to obtain compound **7a** (202 mg, 55%) from **6a** (220 mg, 0.70 mmol). ^{1}H NMR (300MHz, $CDCl_3$) δ 0.89 (t, *J*= 7.2 Hz, 9H), 1.07 (dd, *J*= 8.4, 8.1 Hz, 6H), 1.34 (sext, J= 7.5 Hz, 6H), 1.56 (sext, J= 6.7 Hz, 6H), 3.02 (s, 6H), 6.77 (d, *J*= 8.2 Hz, 2H), 6.78 (s, 1H), 7.27 (d, *J*= 8.0 Hz, 1H), 7.47 (d, *J*= 7.8 Hz, 1H), 7.61 (s, 1H), 7.74 (d, *J*= 9.0 Hz, 2H). MS (DART) *m/z* 527 $[M+H]^+$.

*6-(Tributylstannyl)-2-(4-dimethylaminophenyl)benzofuran (**7b**)*. The procedure used for preparation of **3a** was employed to obtain **7b** (75 mg, 55%) from **6b** (82 mg, 0.35 mmol). ^{1}H NMR (300MHz, $CDCl_3$) δ 0.89 (t, *J*= 7.2 Hz, 9H), 1.09 (dd, *J*= 8.4, 8.1 Hz, 6H), 1.28-1.42 (m, 6H), 1.52-1.68 (m, 6H), 3.03 (s, 6H), 6.77 (d, *J*= 9.3 Hz, 2H), 6.78 (s, 1H), 7.25 (d, *J*= 6.9 Hz, 1H), 7.50 (d, *J*= 7.0 Hz, 1H), 7.59 (s, 1H), 7.74 (d, *J*= 9.3 Hz, 2H). MS (DART) *m/z* 528 $[M+H]^+$.

*5-Iodo-2-(4-dimethylaminophenyl)benzofuran (**5-IBF-NMe$_2$**)*. The procedure used for preparation of 5-IBF-NH_2 was employed to obtain 5-IBF-NMe_2 (65 mg, 47%) from **7a** (200 mg, 0.38 mmol). ^{1}H NMR (300MHz, $CDCl_3$) δ 3.03 (s, 6H), 6.72 (s), 6.78 (d, *J*= 8.1 Hz, 2H), 6.78 (dd, *J*= 8.7, 1.5 Hz, 1H), 7.72 (d, *J*= 9.3 Hz, 1H), 7.83 (d, *J*= 1.5 Hz, 1H). ^{13}C NMR (100MHz, $CDCl_3$) δ 157.8, 153.9, 150.8, 131.5, 128.8, 126.3, 123.0, 117.8, 112.7, 112.1, 97.0, 86.2, 40.3. MS (DART) *m/z* 364 $[M+H]^+$.

*6-Iodo-2-(4-dimethylaminophenyl)benzofuran(**6-IBF-NMe$_2$**)*. The procedure used for preparation of 5-IBF-NH_2 was employed to obtain 6-IBF-NMe_2 (7.0 mg, 39%) from **7b** (25 mg, 0.05 mmol). ^{1}H NMR (300 MHz, $CDCl_3$) δ 3.03 (s, 6H), 6.74 (s, 1H), 6.76 (d, *J* = 8.8 Hz, 2H), 7.25 (s, 1H), 7.48 (dd, *J* = 8.0, 1.2 Hz, 1H), 7.71 (d, *J* = 8.8 Hz, 2H), 7.83 (s, 1H). ^{13}C NMR (100MHz, $CDCl_3$) δ 157.5, 155.0, 150.7, 131.6, 129.6, 126.3, 121.5, 120.0, 117.8, 112.1, 97.7, 85.8, 40.3. MS (DART) *m/z* 364 $[M+H]^+$.

*4-(5-Bromobenzofuran-2-yl)-N-(2-((tert-butyldimethylsilyl)oxy)ethyl) aniline (**8**)*. To a stirred mixture of **2a** (1.00 g, 3.53 mmol) and K_2CO_3 (975 mg, 7.05 mmol) in DMF (20 ml) was added (2-bromoethoxy)-*tert*-butyldimethylsilane (3.78 ml, 17.63 mmol) and heated at 90 °C for 7 h. After the mixture cooled to room temperature, satd NaHCO3aq

(30 mL) was added followed by extraction with $CHCl_3$ (30 mL × 2). The combined organic layers were dried with Na_2SO_4 and evaporated to dryness. The crude product was subjected to chromatographic purification on silica gel using $CHCl_3$/hexane (2:3) to give **8** (628 mg, 40%) as a white powder. ^{1}H NMR (300MHz, $CDCl_3$) δ 0.08 (s, 6H), 0.93 (s, 9H), 3.29 (t, *J*= 5.1 Hz, 2H), 3.85 (t, *J*= 5.7 Hz, 2H), 6.71 (d, *J*= 9.0 Hz, 2H), 6.72 (s, 1H), 7.34-7.25 (m, 2H), 7.63 (d, *J*= 1.5 Hz, 1H), 7.67 (d, *J*= 9.0 Hz, 2H). MS (DART) *m/z* 447 $[M+H]^+$.

N-(2-((tert-butyldimethylsilyl)oxy)ethyl)-4-(5-(tributylstannyl)benzofuran-2-yl) aniline (**9**). The procedure used for preparation of **3a** was employed to obtain compound **9** (319 mg, 43%) from **8** (502 mg, 1.13 mmol). ^{1}H NMR (300MHz, $CDCl_3$) δ 0.08 (s, 6H), 0.89 (t, *J*= 7.5 Hz, 9H), 0.92 (s, 9H), 1.07 (dd, *J*= 8.7, 8.3 Hz, 9H), 1.34 (sext, *J*= 5.7 Hz, 6H), 1.55 (sext, *J*= 6.1 Hz, 6H), 3.27 (t, *J*= 5.4 Hz, 2H), 3.83 (t, *J*= 5.7 Hz, 2H), 4.25 (s, 1H), 6.67 (d, *J*= 9.0 Hz, 2H), 6.77 (s, 1H), 7.28 (d, *J*= 7.4 Hz, 1H), 7.46 (d, *J*= 7.8 H, 1H), 7.60 (s, 1H), 7.68 (d, *J*= 8.7 Hz, 2H). MS (DART) *m/z* 658 $[M+H]^+$.

*4-(5-Iodobenzofuran-2-yl)-N-(2-((tert-butyldimethylsilyl)oxy)ethyl)aniline (**10**).* The procedure used for preparation of 5-IBF-NH_2 was employed to obtain **10** (67 mg, 28%)

from **9** (319 mg, 0.49 mmol). ^{1}H NMR (300MHz, $CDCl_3$) δ 0.08 (s, 6H), 0.93 (s, 9H), 3.28 (t, *J*= 5.1 Hz, 2H), 3.84 (t, *J*= 5.1 Hz, 2H), 4.25 (s, 1H), 6.67 (d, *J*= 8.3 Hz, 2H), 6.70 (s, 1H), 7.26 (d, 8.0 Hz, 1H), 7.47 (dd, *J*= 8.4, 1.3 Hz, 1H), 7.66 (d, *J*= 8.7 Hz, 2H), 7.83 (d, 1.3 Hz, 1H). MS (DART) *m/z* 494 $[M+H]^+$.

*5-Iodo-2-(4-(2-ethanolamino)phenyl)benzofuran (**5-IBF-NHEtOH**)*. To a solution of **10** (62 mg, 0.13 mmol) in THF (3 ml) tetrabutylammonium fluoride in THF (1.26 mL, 1.0 M) was added and reacted at room temperature for 1 h. The reaction mixture was quenched by satd NH_4Claq (15 mL) was added followed by extraction with $CHCl_3$ (20 mL × 2). The combined organic layers were dried with Na_2SO_4 and evaporated to dryness. The crude product was subjected to chromatographic purification on silica gel using $CHCl_3$/MeOH (49:1) to give 5-IBF-NHEtOH (7.0 mg, 17%) as a white powder. ^{1}H NMR (300MHz, $CDCl_3$) δ 3.38 (t, *J*= 5.4 Hz, 2H), 3.89 (t, *J*= 5.4 Hz, 2H), 6.71 (d, *J*= 8.9 Hz, 2H), 6.71 (s, 1H), 7.24 (d, *J*= 7.2 Hz, 1H), 7.47 (dd, *J*= 8.4, 1.3 Hz, 1H), 7.67 (d, *J*= 9.0 Hz, 1H), 7.84 (d, *J*= 1.8 Hz, 2H). ^{13}C NMR (100MHz, $CDCl_3$) δ 157.4, 147.1, 144.6, 134.9, 131.6, 129.4, 120.6, 116.4, 112.9, 112.1, 97.1, 81.6, 53.1, 45.8. MS (DART) *m/z* 380 $[M+H]^+$.

Radiolabeling. The ^{125}I-labeled IBF derivatives were prepared according to the previous study [30]. Briefly, to initiate the reaction, 50 μL of H_2O_2 (3%) was added to a mixture of the tributyltin derivative (50 μg in 50 μL EtOH), [^{125}I]NaI (0.1–0.2 mCi, specific activity = 2200 Ci/mmol), and 1 M HCl (50 μL) in a sealed vial. The reaction was allowed to proceed at room temperature for 3-20 min and was terminated by addition of $NaHSO_3$. After alkalization with 400 μL of 1.0 M NaOH and extraction with ethyl acetate, the extract was dried *via* passage through an anhydrous Na_2SO_4 column, and it was then blown dry with a stream of nitrogen gas. The radioiodinated ligands were purified by HPLC on a Cosmosil C_{18} column at a flow rate of 1.0 mL/min.

Binding assay using rMoPrP aggregates. Expression of the rMoPrP and aggregation of rMoPrP were carried out as described previously[11, 31]. The binding assays of IBF derivatives for rMoPrP aggregates and $A\beta_{1\text{-}42}$ were performed according to our previous studies [17-18]. The adsorption assays were performed by mixing of ^{125}I-IBF derivatives (2.4-3.6 kBq) and an appropriate concentration of rMoPrP aggregates (10-500 nM) in NaCl/HEPES buffer (50 mM HEPES/KOH, 300 mM NaCl, pH 7.5) containing 20% (v/v) DMSO. After incubation for 2 h at room temperature, the mixture was then filtered through Whatman GF/B filters using a Brandel M-24 cell harvester and washed

with the assay buffer 4 times. Each assay tube before filtration and the filters containing the bound ^{125}I ligand were measured by an automatic gamma counter and the bound/free ratio of [^{125}I]ligand was calculated. The saturation assays were performed by mixing an appropriate concentration of ^{125}I-labelled flavonoid derivatives (0.15–8.75 kBq, 6–350 nM) and rMoPrP aggregates or $A\beta_{1\text{-}42}$ (100 nM) in the same buffer with adsorption assays. Incubation, filtration and washing of filters were conducted as same conditions with adsorption assays. The dissociation constant (K_d) and binding capacity (B_{max}) of compounds were estimated by Scatchard analysis using PRISM4 (GraphPad Software Inc., CA, USA). For competitive binding assays, the mixture contained [^{125}I]5-IBF-NHMe (0.02 nM), test compound (4.0 pM–1.0 μ M), and rMoPrP aggregates (100 nM) in the assay buffer. After incubation for 2 h at room temperature, the mixture was filtrated and the filters were measured using the gamma counter. Nonspecific binding was defined in the presence of 10 μ M for nonradioactive of 5-IBF-NHMe. Values for the half maximal inhibitory concentration (IC_{50}) were determined from displacement curves of three independent experiments using PRISM4, and those for the K_i were calculated using the Cheng–Prusoff equation.

Animals. All animals were supplied by Kyudo Co., Ltd. (Saga, Japan). The mBSE

infectious animal experiments were conducted under biosafety level 3 (BSL3) containment in accordance with the institutional guidelines. mBSE-infected and mock-infected mice were treated as previously reported.[32-33] Experiments using animals were conducted in accordance with our institutional guidelines and were approved by the Nagasaki University Animal Care Committee.

Fluorescence staining immunohistochemical analysis of mBSE-infected and mock-infected mouse brain sections. The animals used for the *in vitro* experiments were exsanguinated *via* transcardial perfusion with saline under ether anesthesia, and their brains were subsequently excised and frozen in an EtOH ice bath. The frozen blocks were sliced into 10-μm-thick serial sections. The sections were incubated with a 20% DMSO solution (100 μM) of IBF derivatives for 24 h. Each section was washed with 20 % DMSO twice. The fluorescence images were obtained using an Eclipse 80i microscope (Nikon Corp., Tokyo, Japan) with a B-2A filter set (excitation, 450–490 nm; dichromic mirror, 505 nm; longpass filter, 520 nm). Then, the deposits of PrP^{Sc} in the serial sections were detected by fluorescence staining by ThT (50 μM) or immunohistochemical staining using SAF32 anti-PrP antibody as described in our previous papers.[17-18]

***In vitro* autoradiography in mouse brain sections.** Each brain section was incubated in 20% (v/v) DMSO solution containing [^{125}I]ligand (20.8 kBq, 0.02 nM) for 1 h. The slices were rinsed for 2 min, three times each, with 50% (v/v) DMSO solution, and subsequently dipped into cold water for 20 s. The sections were dried under a steam of cold air and placed in contact with imaging plates (BAS-MS 2040; GE Health Care) for 24 h. Distribution of radioactivity on the plates were analysed using the Fluoro Image Analyzer (FLA5100; GE Health Care). Thereafter, serial sections were incubated with a 50% DMSO solution of Th-S (50 μM) for 24 hours. The sections were washed in 50% DMSO for 5 min twice.

***In vivo* biodistribution in normal mice.** A saline solution (100 μL) of ^{125}I-IBF derivatives (7.4-14.8 kBq) containing DMSO (20 μL) was injected directly into the tail vein of ddY mice (male, 5 weeks old, 20-25 g). The mice were sacrificed at 2, 10, 30, 60 and 180 min post injection. The organs of interest were removed and weighed, and the radioactivity was measured using a gamma counter (PerkinElmer, 2470 WIZARD^2).

CNS PET MPO score calculation. ClogP and TPSA were calculated using a ChemBioDraw Ultra 13.0. ClogD and pKa were calculated using a SPARK on line

calculator. The CNS MPO score calculation has been carried out according to the literature.[24]

Acknowledgements

Financial supports were provided by the Grant-in-Aid for Scientific Research (B) (Grant No. 21390348) and Grant-in-Aid for Exploratory Research (Grant No. 20659192) from the Japan Society for the Promotion of Science (JSPS), GSK Japan Research Grant 2015 and a grant from Takeda Science Foundation.

AUTHOR INFORMATION

Corresponding Authors

*E-mail: t-fuchi@nagasaki-u.ac.jp.

*E-mail: morio@nagasaki-u.ac.jp.

ORCID

Takeshi Fuchigami: 0000-0001-8141-1212

Notes

The authors declare no competing financial interest.

Reference

1. Aguzzi, A.; Polymenidou, M., Mammalian prion biology: one century of evolving concepts. *Cell* **2004,** *116* (2), 313-327 DOI https://doi-org.stanford.idm.oclc.org/10.1016/S0092-8674(03)01031-6.

2. Knight, R., Chapter Thirteen - Infectious and Sporadic Prion Diseases. *Prog Mol Biol Transl Sci* **2017**, 150, 293-318 DOI 10.1016/bs.pmbts.2017.06.010.

3. Budka, H., Neuropathology of prion diseases. *Br Med Bull* **2003,** *66*, 121-130 DOI 10.1093/bmb/dg66.121.

4. Aguzzi, A.; Calella, A. M., Prions: protein aggregation and infectious diseases. *Physiol Rev* **2009,** *89* (4), 1105-1152 DOI 10.1152/physrev.00006.2009.

5. Collinge, J., Molecular neurology of prion disease. *J Neurol Neurosurg Psychiatry* **2005,** *76* (7), 906-919 DOI 10.1136/jnnp.2004.048660.

6. AM, T. I.; Adlard, P. A.; Finkelstein, D. I.; Lewis, V.; Biggi, S.; Biasini, E.; Collins, S. J., Acute Neurotoxicity Models of Prion Disease. *ACS Chem Neurosci* **2018,** *9* (3), 431-445 DOI 10.1021/acschemneuro.7b00517.

7. Kraus, A.; Groveman, B. R.; Caughey, B., Prions and the potential transmissibility of protein misfolding diseases. *Annu Rev Microbiol,* **2013,** *67*, 543-564 DOI 10.1146/annurev-micro-092412-155735.

8. Shah, S. Z. A.; Zhao, D.; Hussain, T.; Yang, L., The Role of Unfolded Protein Response and Mitogen-Activated Protein Kinase Signaling in Neurodegenerative Diseases with Special Focus on Prion Diseases. *Front Aging Neurosci* **2017,** *9*, 120 DOI 10.3389/fnagi.2017.00120.

9. Puig, B.; Altmeppen, H. C.; Glatzel, M., Misfolding leads the way to unraveling signaling pathways in the pathophysiology of prion diseases. *Prion* **2016,** *10* (6), 434-443 DOI 10.1080/19336896.2016.1244593.

10. Puoti, G.; Bizzi, A.; Forloni, G.; Safar, J. G.; Tagliavini, F.; Gambetti, P., Sporadic human prion diseases: molecular insights and diagnosis. *Lancet Neurol* **2012,** *11* (7), 618-628 DOI 10.1016/S1474-4422(12)70063-7.

11. Atarashi, R.; Satoh, K.; Sano, K.; Fuse, T.; Yamaguchi, N.; Ishibashi, D.; Matsubara, T.; Nakagaki, T.; Yamanaka, H.; Shirabe, S.; Yamada, M.; Mizusawa, H.; Kitamoto, T.; Klug, G.; McGlade, A.; Collins, S. J.; Nishida, N., Ultrasensitive human prion detection in cerebrospinal fluid by real-time quaking-induced conversion. *Nat Med* **2011,** *17* (2), 175-178 DOI 10.1038/nm.2294.

12. Bongianni, M.; Orrù, C.; Groveman, B. R.; Sacchetto, L.; Fiorini, M.; Tonoli, G.; Triva, G.; Capaldi, S.; Testi, S.; Ferrari, S.; Cagnin, A.; Ladogana, A.; Poleggi, A.; Colaizzo, E.; Tiple, D.; Vaianella, L.; Castriciano, S.; Marchioni, D.; Hughson, A. G.;

Imperiale, D.; Cattaruzza, T.; Fabrizi, G. M.; Pocchiari, M.; Monaco, S.; Caughey, B.; Zanusso, G., Diagnosis of human prion disease using real-time quaking-induced conversion testing of olfactory mucosa and cerebrospinal fluid samples. *JAMA Neurol* **2017,** *74* (2), 155-162 DOI 10.1001/jamaneurol.2016.4614.

13. Rambaran, R. N.; Serpell, L. C., Amyloid fibrils: abnormal protein assembly. *Prion* **2008,** *2* (3), 112-117.

14. Letourneau-Guillon, L.; Wada, R.; Kucharczyk, W., Imaging of prion diseases. *Journal of magnetic resonance imaging : J Magn Reson Imaging* **2012,** *35* (5), 998-1012 DOI 10.1002/jmri.23504.

15. Deters, K. D.; Risacher, S. L.; Yoder, K. K.; Oblak, A. L.; Unverzagt, F. W.; Murrell, J. R.; Epperson, F.; Tallman, E. F.; Quaid, K. A.; Farlow, M. R.; Saykin, A. J.; Ghetti, B., [(11)C]PiB PET in Gerstmann-Straussler-Scheinker disease. *Am J Nucl Med Mol Imaging* **2016,** *6* (1), 84-93.

16. Okamura, N.; Shiga, Y.; Furumoto, S.; Tashiro, M.; Tsuboi, Y.; Furukawa, K.; Yanai, K.; Iwata, R.; Arai, H.; Kudo, Y.; Itoyama, Y.; Doh-ura, K., In vivo detection of prion amyloid plaques using [(11)C]BF-227 PET. *Eur J Nucl Med Mol Imaging* **2010,** *37* (5), 934-941 DOI 10.1007/s00259-009-1314-1317.

17. Fuchigami, T.; Yamashita, Y.; Kawasaki, M.; Ogawa, A.; Haratake, M.; Atarashi,

R.; Sano, K.; Nakagaki, T.; Ubagai, K.; Ono, M.; Yoshida, S.; Nishida, N.; Nakayama, M., Characterisation of radioiodinated flavonoid derivatives for SPECT imaging of cerebral prion deposits. *Sci Rep* **2015,** 5 DOI 10.1038/srep18440.

18. Kawasaki, M.; Fuchigami, T.; Kobashi, N.; Nakagaki, T.; Sano, K.; Atarashi, R.; Yoshida, S.; Haratake, M.; Nishida, N.; Nakayama, M., Development of radioiodinated acridine derivatives for in vivo imaging of prion deposits in the brain. *Bioorg Med Chem* **2017,** *25* (3), 1085-1093 DOI 10.1016/j.bmc.2016.12.020.

19. Ono, M.; Kung, M. P.; Hou, C.; Kung, H. F., Benzofuran derivatives as Abeta-aggregate-specific imaging agents for Alzheimer's disease. *Nucl Med Biol* **2002,** *29* (6), 633-642 DOI 10.1016/S0969-8051(02)00326-8.

20. Ono, M.; Kawashima, H.; Nonaka, A.; Kawai, T.; Haratake, M.; Mori, H.; Kung, M. P.; Kung, H. F.; Saji, H.; Nakayama, M., Novel benzofuran derivatives for PET imaging of beta-amyloid plaques in Alzheimer's disease brains. *J Med Chem* **2006,** *49* (9), 2725-2730 DOI 10.1021/jm051176k.

21. Ono, M., Development of positron-emission tomography/single-photon emission computed tomography imaging probes for in vivo detection of beta-amyloid plaques in Alzheimer's brains. *Chem Pharm Bull (Tokyo)* **2009,** *57* (10), 1029-1039 DOI 10.1248/cpb.57.1029.

22. Pike, V. W., PET radiotracers: crossing the blood-brain barrier and surviving metabolism. *Trends Pharmacol Sci* **2009,** *30* (8), 431-440 DOI 10.1016/j.tips.2009.05.005.

23. Waterhouse, R. N., Determination of lipophilicity and its use as a predictor of blood-brain barrier penetration of molecular imaging agents. *Mol Imaging Biol* **2003,** *5* (6), 376-389 DOI 10.1016/j.mibio.2003.09.014.

24. Zhang, L.; Villalobos, A.; Beck, E. M.; Bocan, T.; Chappie, T. A.; Chen, L.; Grimwood, S.; Heck, S. D.; Helal, C. J.; Hou, X.; Humphrey, J. M.; Lu, J.; Skaddan, M. B.; McCarthy, T. J.; Verhoest, P. R.; Wager, T. T.; Zasadny, K., Design and selection parameters to accelerate the discovery of novel central nervous system positron emission tomography (PET) ligands and their application in the development of a novel phosphodiesterase 2A PET ligand. *J Med Chem* **2013,** *56* (11), 4568-4579 DOI 10.1021/jm400312y.

25. Wager, T. T.; Hou, X.; Verhoest, P. R.; Villalobos, A., Moving beyond rules: the development of a central nervous system multiparameter optimization (CNS MPO) approach to enable alignment of druglike properties. *ACS Chem Neurosci* **2010,** *1* (6), 435-449 DOI 10.1021/cn100008c.

26. Ono, M.; Cheng, Y.; Kimura, H.; Cui, M.; Kagawa, S.; Nishii, R.; Saji, H., Novel

^{18}F-labeled benzofuran derivatives with improved properties for positron emission tomography (PET) imaging of beta-amyloid plaques in Alzheimer's brains. *J Med Chem* **2011,** *54* (8), 2971-2979 DOI 10.1021/jm200057u.

27. Iwasaki, Y.; Yoshida, M.; Hashizume, Y.; Kitamoto, T.; Sobue, G., Clinicopathologic characteristics of sporadic Japanese Creutzfeldt-Jakob disease classified according to prion protein gene polymorphism and prion protein type. *Acta Neuropathol* **2006,** *112* (5), 561-571 DOI 10.1007/s00401-006-0111-7.

28. Ishizawa, K.; Mitsufuji, T.; Shioda, K.; Kobayashi, A.; Komori, T.; Nakazato, Y.; Kitamoto, T.; Araki, N.; Yamamoto, T.; Sasaki, A., An autopsy report of three kindred in a Gerstmann-Straussler-Scheinker disease P105L family with a special reference to prion protein, tau, and beta-amyloid. *Brain Behav* **2018,** *8* (10), e01117 DOI 10.1002/brb3.1117.

29. Thal, D. R.; Rub, U.; Orantes, M.; Braak, H., Phases of A beta-deposition in the human brain and its relevance for the development of AD. *Neurology* **2002,** *58* (12), 1791-1800 DOI 10.1212/WNL.58.12.1791.

30. Fuchigami, T.; Kobashi, N.; Haratake, M.; Kawasaki, M.; Nakayama, M., Synthesis and biological evaluation of radioiodinated quinacrine-based derivatives for SPECT imaging of Aβ plaques. *Eur J Med Chem* **2013,** *60*, 469-478 DOI

10.1016/j.ejmech.2012.12.020.

31. Atarashi, R.; Moore, R. A.; Sim, V. L.; Hughson, A. G.; Dorward, D. W.; Onwubiko, H. A.; Priola, S. A.; Caughey, B., Ultrasensitive detection of scrapie prion protein using seeded conversion of recombinant prion protein. *Nat Methods* **2007,** *4* (8), 645-650 DOI 10.1038/nmeth1066.

32. Fujihara, A.; Atarashi, R.; Fuse, T.; Ubagai, K.; Nakagaki, T.; Yamaguchi, N.; Ishibashi, D.; Katamine, S.; Nishida, N., Hyperefficient PrP Sc amplification of mouse-adapted BSE and scrapie strain by protein misfolding cyclic amplification technique. *FEBS J* **2009,** *276* (10), 2841-2848 DOI 10.1111/j.1742-4658.2009.07007.x.

33. Nakagaki, T.; Satoh, K.; Ishibashi, D.; Fuse, T.; Sano, K.; Kamatari, Y. O.; Kuwata, K.; Shigematsu, K.; Iwamaru, Y.; Takenouchi, T.; Kitani, H.; Nishida, N.; Atarashi, R., FK506 reduces abnormal prion protein through the activation of autolysosomal degradation and prolongs survival in prion-infected mice. *Autophagy* **2013,** *9* (9), 1386-1394 DOI 10.4161/auto.25381.

Table of Contents

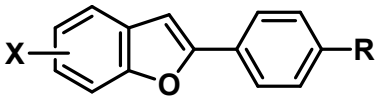

X= 5-^{125}I, 6-^{125}I
R= NH_2, NHMe, NMe_2, $NHCH_2CH_2OH$

[^{125}I]5-IBF-NHMe: X= 5-^{125}I, R= NHMe

K_d= 12.3 nM for rMoPrP aggregates